

## Article

# Integration of HEC-RAS and HEC-HMS with GIS in Flood Modeling and Flood Hazard Mapping

İsmail Bilal Peker <sup>1</sup>, Sezar Gülbaz <sup>1</sup>, Vahdettin Demir <sup>2,\*</sup>, Osman Orhan <sup>3</sup> and Neslihan Beden <sup>4,\*</sup>

<sup>1</sup> Department of Civil Engineering, Istanbul University-Cerrahpaşa, Avcılar, Istanbul 34320, Türkiye; pekerbilal@iuc.edu.tr (İ.B.P.); sezarg@iuc.edu.tr (S.G.)

<sup>2</sup> Department of Civil Engineering, KTO Karatay University, Konya 42020, Türkiye

<sup>3</sup> Department of Geomatic Engineering, Mersin University, Mersin 33110, Türkiye; osmanorhan@mersin.edu.tr

<sup>4</sup> Department of Meteorological Engineering, Özdemir Bayraktar Faculty of Aeronautics and Astronautics, University of Samsun, Samsun 55000, Türkiye

\* Correspondence: vahdettin.demir@karatay.edu.tr (V.D.); neslihan.beden@samsun.edu.tr (N.B.); Tel.: +90-546-496-88-05 (V.D.)

**Abstract:** Floods are among the most devastating disasters in terms of socio-economics and casualties. However, these natural disasters can be managed and their effects can be minimized by flood modeling performed before the occurrence of a flood. In this study, flood modeling was developed for the Göksu River Basin, Mersin, Türkiye. Flood hazard and risk maps were prepared by using GIS, HEC-RAS, and HEC-HMS. In hydraulic modeling, Manning's  $n$  values were obtained from 2018 CORINE data, return period flow rates (Q25, Q50, Q100, Q500) were obtained from HEC-HMS, and the application was carried out on a 5 m resolution digital surface model. In the study area, the water depths could reach up to 10 m, and water speeds were approximately 0.7 m/s. Considering these values and the fact that the study area is an urban area, hazard maps were obtained according to the UK Department for Environment, Food and Rural Affairs (DEFRA) method. The results indicated that possible flood flow rates from Q25 to Q500, from 1191.7 m<sup>3</sup>/s to 1888.3 m<sup>3</sup>/s, were detected in the study area with HEC-HMS. Flooding also occurred under conditions of the Q25 flow rate (from 4288 km<sup>2</sup> to 5767 km<sup>2</sup>), and the impacted areas were classified as extremely risky by the DEFRA method.

**Keywords:** HEC-HMS; HEC-RAS; Göksu River Basin; flood modeling; flood hazard



**Citation:** Peker, İ.B.; Gülbaz, S.; Demir, V.; Orhan, O.; Beden, N. Integration of HEC-RAS and HEC-HMS with GIS in Flood Modeling and Flood Hazard Mapping. *Sustainability* **2024**, *16*, 1226. <https://doi.org/10.3390/su16031226>

Academic Editor: Pingping Luo

Received: 3 December 2023

Revised: 19 January 2024

Accepted: 29 January 2024

Published: 1 February 2024



**Copyright:** © 2024 by the authors. Licensee MDPI, Basel, Switzerland. This article is an open access article distributed under the terms and conditions of the Creative Commons Attribution (CC BY) license (<https://creativecommons.org/licenses/by/4.0/>).

## 1. Introduction

Disasters can be caused by many different kinds of hazards, namely floods, landslides, earthquakes, wildfires, and droughts. Hazards are of natural, technological, or anthropogenic origin that may cause loss of life and property, damage, and harm if they occur [1]. Disaster is defined as the disruption of the existing societal order and conditions of the living environment as a consequence of the occurrence of hazards, leading to physical, economic, and social damages at a level beyond a society's adaptive capacity. According to The Emergency Events Database (EM-DAT) [2], it has been stated that 9865 hazards causing natural disasters have been recorded on a global scale (Africa, Americas, Asia, Europe, and Oceania) between 2000 and 2023. Additionally, 3992 (40%) of these natural disasters were recorded as flood-related during this period.

Among disasters, floods are one of the most common and destructive phenomena observed worldwide and are occurring more frequently due to global warming and climate change [3,4]. Population growth, urbanization, and industrialization have caused vegetation destruction, soil loss, and increases in artificial and impermeable surfaces in urban areas [5,6]. In addition, interfering with the natural flow in riverbeds can potentially cause ordinary natural events to turn into flood disasters. The destructive effect of floods is more severe in cities with inadequate permeable surfaces and scarce underground drainage

channels [7]. Flood control and prevention strategies are desperately needed because floods can cause massive and irreversible damage to agriculture, transportation, bridges, and other elements of urban infrastructure [8,9]. Although it is very difficult to prevent flood disasters in the moment, their impact can be significantly reduced if potential flood areas are identified and adequate precautions are taken in these areas. In addition, as a result of the climate crisis, identifying flood-prone locations and assessing the linkages between disasters and the environment have become essential and urgent needs in urban flood risk management. Therefore, studies that determine potential flood impact areas and disaster damage using techniques such as geographic information systems [10], remote sensing [11], and hydrological modeling [12] are crucial for managers and decision makers.

Compared to other natural disasters, many more people are directly or indirectly affected by extreme weather events such as drought and flood. Floods are the most devastating among these natural disasters in terms of socio-economics and deaths. If the cross-sectional capacity is exceeded at various points along a river route, floods may cause severe damage in basins and coastal areas. Therefore, determining how to predict flood risk and what precautions to take is crucial. Determination of the volume of surface runoff caused by precipitation is critical in determining the storage capacity of reservoirs and estimating the probability of flooding. It is essential to obtain timely and reliable flood information and accurate data about flood risks by interpreting flood maps to prevent possible post-event disasters and reduce damages in flood areas. The first step in obtaining various flood maps and risk maps is to perform flood modeling, such as hydrological and hydraulic modeling [13]. Numerical models are essential in developing a hydraulic model and applying hydraulic analysis of river beds using the HEC-RAS program, which is a perfect choice for performing hydraulic calculations in both natural and structural channel systems [14]. In recent years, the integrated use of geographic information systems (GIS) with hydrological and hydraulic modeling has significantly improved numerical flood modeling. The GIS environment can extract the hydrological variables from a digital elevation model (DEM) with good accuracy, such as watershed shapes, path lengths, flow directions, delineations, and slopes. The HEC-GeoRAS, a tool of HEC-RAS, uses mathematical equations to calculate riverbed coefficients based on the river water flow rate, the amount of drainage, and the rate at which water enters the soil. Numerical models allow researchers to evaluate floods quantitatively and evaluate flood risks and other related risks qualitatively. Flood modeling is a technical method for obtaining high-accuracy information regarding important flood factors such as runoff, storage, and velocity.

The Hydrologic Engineering Center's Hydrologic Modeling System (HEC-HMS) model [15], developed by the US Army Corps of Engineers, has applications in various hydrological simulations, including urban flood analysis, flood frequency assessment, flood warning system planning, reservoir spillway capacity evaluation, and stream restoration planning. There are many studies conducted with HEC-HMS in different parts of the world in urban areas [16–20], agricultural areas [21,22], wetlands [23], arid or semi-arid regions [22,24], and tropical regions [25]. HEC-HMS enables event-based flood analysis as well as the capability for continuous model simulations [26]. Specifically, the model has been used in many successful studies to predict flood peak discharges and hydrographs [27,28]. There have been many studies conducted using a combination of HEC-RAS and HEC-HMS in the literature.

The Hydrologic Engineering Center's Hydrologic Modeling System (HEC-HMS) and River Analysis System (HEC-RAS) were integrated by Gül et al. to investigate the feasibility of constructing a planned dam in Türkiye's Bostanlı basin [29]. In order to simulate floods in the Khoshke Rudan River in the Iranian province of Fars, Hashemyan et al. merged the HEC-HMS and HEC-RAS models in a GIS [30]. Yamani et al. evaluated the susceptibility of flooded areas in arid sections of Ghardaia city by using HEC-HMS and HEC-RAS [31]. Mai and de Smedt integrated the hydrological and hydraulic models for flood prediction in Vietnam [32]. Namai et al. produced inundation maps using HEC-RAS and HEC-HMS models in Awash Bello flood plain, Upper Awash River Basin, Ethiopia [33].

This paper focuses on the simulation of the occurrence of floods in the Göksu River Basin, which has flooded several times in the past. In this study, HEC-HMS, HEC-RAS, and GIS models were integrated in flood modeling and flood hazard mapping of the Göksu River Basin. For this purpose, various return intervals from intensity–duration–frequency (IDF) curves were used in the hydrological model: 25, 50, 100, and 500 years. Moreover, hydraulic 2D flow modeling was performed with HEC-RAS. Manning’s “n” values, based on CORINE data, were determined, and flood propagation scenarios of flow hydrographs obtained from HEC-HMS were mapped. Finally, flood hazard maps were obtained by using the flood depth–velocity and the UK Department for Environment, Food and Rural Affairs (DEFRA) method.

## 2. Materials and Methods

### 2.1. Study Area: Göksu River Basin

The Göksu River Basin is a part of the East Mediterranean Basin as part of Türkiye’s 25 main basins (Figure 1). Göksu River flows through Antalya, Konya, Karaman, and Mersin provinces and flows into the Mediterranean in the south of Silifke district of Mersin province. The length of the Göksu River is 260 km, and its basin area is approximately 10,000 km<sup>2</sup>. It has two branches of approximately the same length: the northern branch is Gökçay, and the southern branch is Gökdere, both of which originate from the Geyik Mountains in the Taurus Mountains. After passing Karaman–Ermenek, these two branches unite in the south of Mut and are named Göksu and then flow into the Mediterranean in the delta known as Paradeniz, south of Silifke. The average altitude of the basin is about 1300 m, varying from sea level to 2870 m. In the study region, where the Mediterranean climate prevails, heavy storms are observed with orographic effects, especially in the coastal areas [34–36].

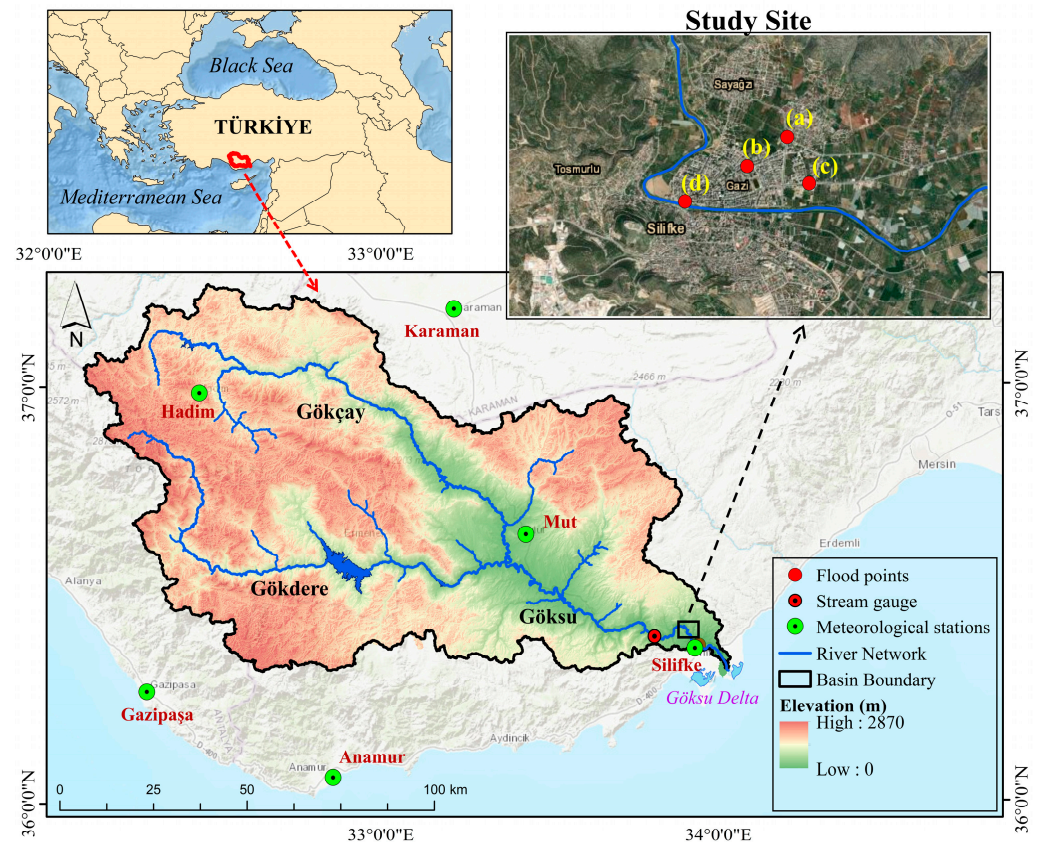


**Figure 1.** Göksu River Basin and the study site, with the location of flood points a, b, c, d.

In this study, the Göksu River Basin was modeled using HEC-HMS hydrological processes. Then, the Silifke city area, in the region close to the basin's outlet, was specifically examined as a site description for flood analysis as shown in Figure 1.

In Silifke, the present study area, there have been many flood events in the past that caused loss of life and property [37,38]. Records of the State Hydraulic Works (DSI) and Disaster and Emergency Management Presidency (AFAD), two institutions related to floods in Türkiye, reveal these historical events. When the records determined by DSI are examined, 17 different flood events can be seen in the region for Silifke alone as of 2006. The critical importance of the region in terms of floods is emphasized by the Silifke flood on 7 March 2004, which was recorded in a study as a flood with a 500-year return period [36]. The points a, b, c, d shown in Figure 1 indicated the locations of these flood events. This record is listed as one of the most severe flood events in Türkiye [39] and appears to have caused serious damage to urban and agricultural areas (Figure 2). In addition, other historical flood events have occurred based on AFAD records. For example, a heavy storm in Mersin's Silifke District on 5 November 2011 led to the inundation of numerous vehicles beneath floodwaters, caused by overflow of the stream bed.



**Figure 2.** The effects of the extremely severe flood experienced in Silifke on 7 March 2004 on (a) agriculture areas, (b) urban regions, and (c,d) hydraulic structures [36].

## 2.2. HEC-HMS Model Data and Base Model Setup

This study utilized geospatial and meteorological data for the HEC-HMS model setup. The properties of all input data used are given in Table 1.

**Table 1.** Properties of input data used in the HEC-HMS model.

Data	Data Type	Source	Source Link	Resolution/ Time Step	Intended Purpose (s)
DEM	Geospatial	SRTM	<a href="https://earthexplorer.usgs.gov/">https://earthexplorer.usgs.gov/</a> (accessed on 9 June 2023)	30 m	Basin delineation
Land use		CORINE 2018	<a href="https://land.copernicus.eu/">https://land.copernicus.eu/</a> (accessed on 9 June 2023)	100 m	Definition of river network CN grid generation (land-use type)
Soil type		HYSOGs250m	<a href="https://daac.ornl.gov/">https://daac.ornl.gov/</a> (accessed on 9 June 2023)	250 m	CN grid generation (hydrologic soil group)
Rainfall	Meteorological	TSMS	<a href="https://www.mgm.gov.tr/">https://www.mgm.gov.tr/</a> (accessed on 9 June 2023)	Intensity–Duration–Frequency (IDF)	Definition of rainfall for 25, 50, 100, and 500 yr return period

Data from the Shuttle Radar Topography Mission (SRTM)'s 30 m resolution digital elevation model (DEM) [40] were employed to delineate the Göksu River Basin into subbasins and to establish the stream network.

To facilitate the “time of concentration ( $T_c$ )” calculation for the hydrological model, the curve number (CN) values were computed. To achieve this, an overlay of Coordination of Information on the Environment 2018 (CORINE 2018) land-use data [41] and ORNL DAAC (Oak Ridge National Laboratory Distributed Active Archive Center) HYSOGs250m soil-type data [42] was performed. Land-use types and Hydrologic soil group (C and D) are shown in Figure 3a and Figure 3b, respectively. Also, Figure 4 presents the CN grids resulting from overlapping.

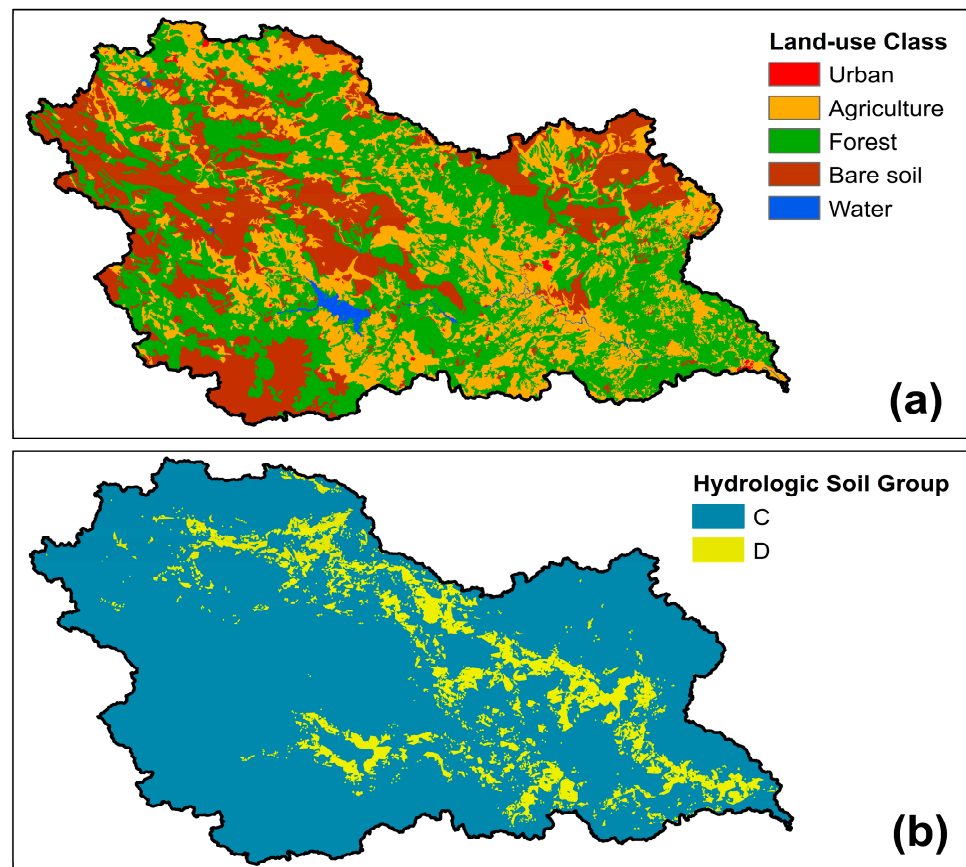


**Figure 3.** (a) Land-use class and (b) soil-type map of Göksu River Basin.

The CN grid map was created using ArcHydro [43], an ArcGIS plugin used to combine land-use and soil-type data in the same coordinate. In the overlapping process, CN values were constituted for each combination of land use and soil type. Then, a CN map was output as raster data covering the entire basin. To meet the HEC-HMS input requiring a single average CN value for each subbasin, the next step involved calculating the average CN values within the boundaries of each subbasin. This provided a representation of CN values for use in hydrological modeling in the context of the basin.

Subsequently, the “lag time” for each subbasin was calculated. The final step involved determining the time of concentration values based on the calculated CN and lag time values. Equation (1) [44] was used to calculate the time of concentration. The average CN values, the time of concentration ( $T_c$ ), and lag time values for each subbasin based on Equation (1) are presented in Table 2.

$$T_c = \frac{l^{0.8}(S+1)^{0.7}}{1140Y^{0.5}} \quad Lag = 0.6T_c \quad (1)$$

where  $L = \text{lag [T]}$ ,  $T_c = \text{time of concentration [T]}$ ,  $l = \text{flow length [L]}$ ,  $Y = \text{basin slope [\%]}$ ,  $S = \text{maximum potential retention [L]}$ ,  $S = (1000/\text{CN}) - 10$ , ( $0 < \text{CN} < 100$ ).

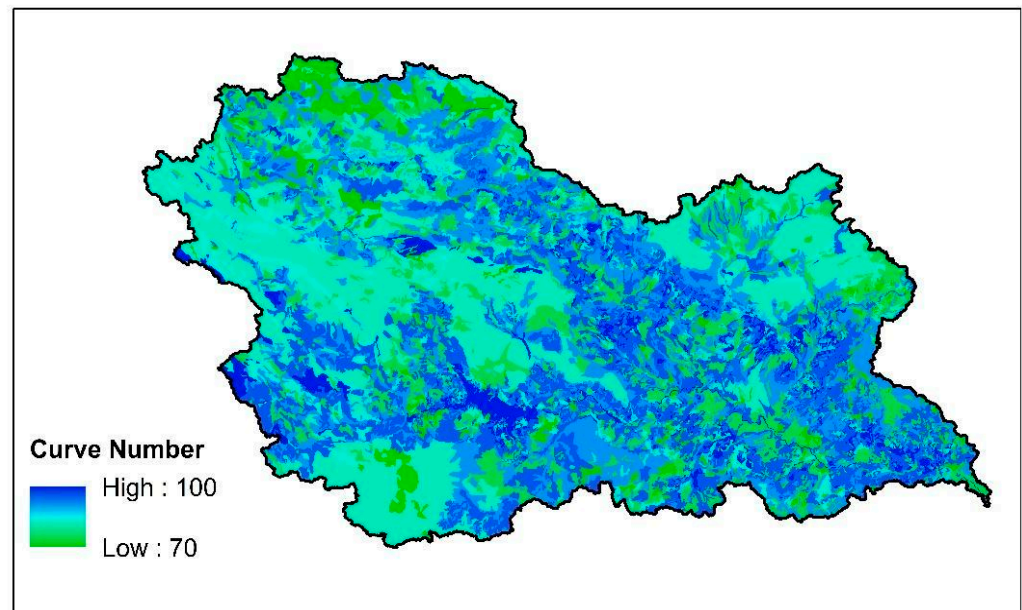


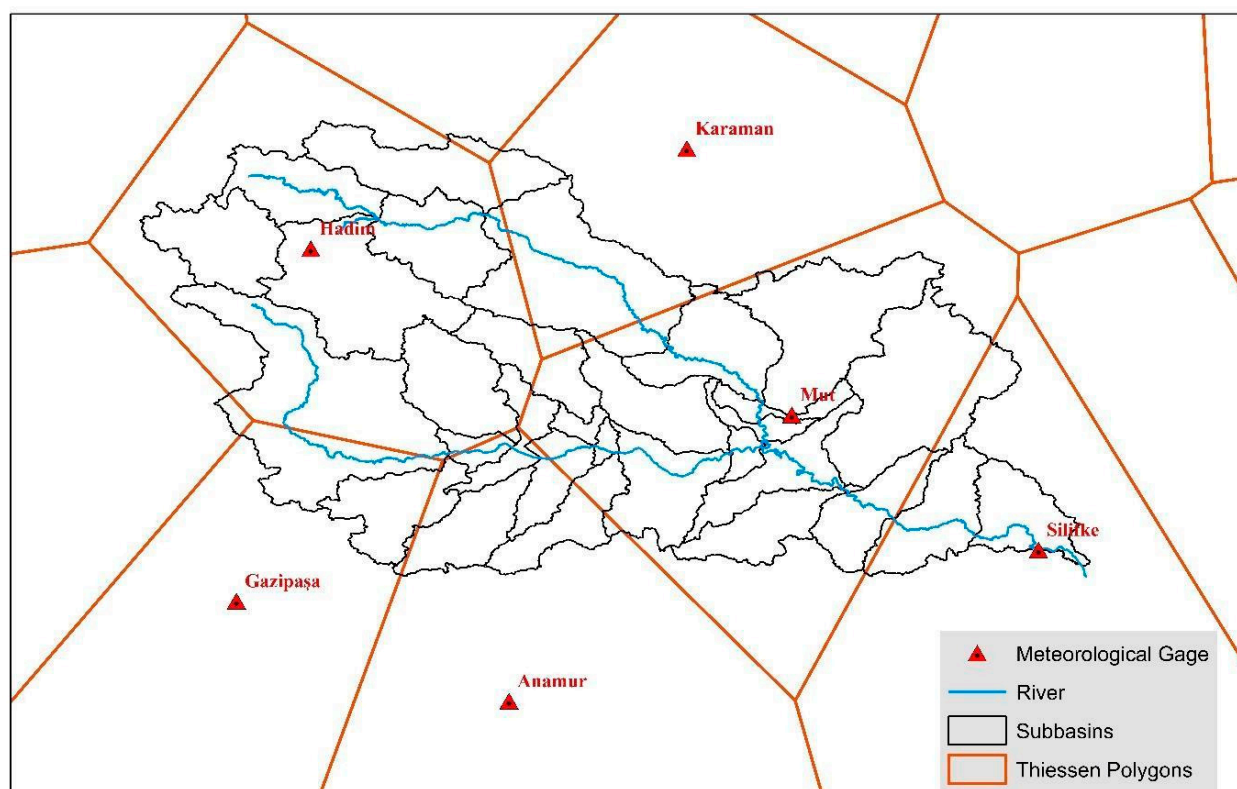
Figure 4. Curve number grids of Göksu River Basin.

Table 2. Calculation table of CN, time of concentration, lag time, and subbasin characteristics.

Subbasin	Reach	Average CN	Longest Flowpath Length (km)	Basin Slope (m/m)	Maximum Potential Retention S	Basin Slope (%)	Time of Concentration Tc (h)	Lag Time (h)	Meteorological Station (TSMS)
S1		79.06	55.52	0.18	2.65	17.55	8.23	4.94	Hadim
S10	R8	85.86	48.66	0.22	1.65	22.04	5.27	3.16	Anamur
S11		80.39	50.67	0.23	2.44	23.26	6.37	3.82	Gazipaşa
S12		83.15	53.51	0.25	2.03	24.55	5.92	3.55	Anamur
S13		85.24	47.36	0.24	1.73	23.80	5.08	3.05	Mut
S14	R14	84.49	14.44	0.27	1.84	27.08	1.89	1.13	Mut
S15	R16	81.44	51.10	0.23	2.28	23.17	6.21	3.73	Hadim
S16	R18	90.73	0.18	0.07	1.02	7.23	0.09	0.05	Hadim
S17	R9	83.68	39.00	0.29	1.95	29.30	4.13	2.48	Hadim
S18		87.43	22.05	0.36	1.44	35.73	2.08	1.25	Anamur
S19	R7	83.11	33.11	0.21	2.03	20.68	4.40	2.64	Anamur
S2		81.53	46.04	0.28	2.27	27.70	5.21	3.13	Hadim
S20	R10	85.20	76.79	0.31	1.74	31.32	6.53	3.92	Karaman
S21	R6	87.06	34.36	0.28	1.49	27.72	3.41	2.04	Anamur
S22	R5	87.02	13.33	0.37	1.49	36.74	1.39	0.83	Mut
S23	R4	85.95	40.73	0.26	1.63	26.02	4.20	2.52	Mut
S24	R3	85.84	19.22	0.19	1.65	18.67	2.73	1.64	Mut
S25	R11	86.39	46.31	0.24	1.58	24.14	4.75	2.85	Mut
S26	R12	85.49	27.65	0.18	1.70	18.10	3.75	2.25	Mut
S27	R13	84.99	27.82	0.13	1.77	13.47	4.45	2.67	Mut
S28	R2	84.29	59.70	0.18	1.86	18.08	7.25	4.35	Mut
S29	R1	77.24	4.76	0.07	2.95	7.43	1.87	1.12	Mut
S3		81.99	64.87	0.28	2.20	27.95	6.73	4.04	Hadim
S30	R15	84.97	34.27	0.22	1.77	21.91	4.12	2.47	Mut
S31	R17	85.52	41.22	0.29	1.69	29.30	4.06	2.43	Silifke
S32	R19	85.31	44.43	0.21	1.72	21.11	5.11	3.07	Silifke
S4		82.43	61.04	0.21	2.13	20.95	7.30	4.38	Mut
S5		85.43	105.81	0.35	1.70	34.55	7.96	4.78	Hadim
S6		83.55	87.58	0.21	1.97	21.02	9.37	5.62	Mut
S7		82.46	42.11	0.24	2.13	23.54	5.11	3.07	Hadim
S8		83.72	49.91	0.25	1.94	25.48	5.39	3.24	Hadim
S9		84.60	52.38	0.24	1.82	24.37	5.56	3.34	Mut

Next, rainfall data were defined after the delineation process. For this, rainfall data were gathered from observations by the Turkish State Meteorological Service (TSMS), Republic of Türkiye Ministry of Environment, Urbanization, and Climate Change. These data include six different meteorological stations representing the basin. The locations of

these stations, named Mut, Karaman, Anamur, Silifke, Gazipasa, and Hadim, are shown in Figure 5. By employing Thiessen polygons, this study was able to create discrete areas for each subbasin, which facilitated the allocation of data and parameters specific to each subbasin in the subsequent analysis and modeling processes. This spatial representation helps to improve the accuracy and efficiency of the hydrological and other environmental assessments conducted within the Göksu River Basin. The matching of the subbasins represented by the meteorological stations is given in Table 2.



**Figure 5.** Location of meteorological and stream gauges with Thiessen polygons for Göksu River Basin.

Also, the intensity–duration–frequency (IDF) curves of 25-, 50-, 100-, and 500-year rainfall data for the six meteorological stations are shown in Figure 6.

### 2.3. HEC-HMS Model Runs and Parameter Adjustment

HEC-HMS offers various approaches to simulate the rainfall runoff processes within a basin that support parameter-based models. The model has three main components, namely the basin model, the meteorological model, and control specifications. It allows users to choose from a variety of different methods. In our basin model, “SCS Curve Number” for the loss method, “Clark Unit Hydrograph” for the transform method, and “Lag” for the routing method were preferred. The values of CN,  $T_c$ , and lag time for each subbasin, as presented in Table 2, were employed to ascertain the parameters for the respective methods. In a meteorological component, precipitation data as IDF curves were inputted. The control specifications section defines the start and end times of the desired simulation period, in our study, the duration along the flood hydrograph. In summary, the HEC-HMS modeling process is illustrated in the flowchart in Figure 7.

Model simulations of flow rates for return periods of 500-year, 100-year, and 50-year data were conducted, and a parameter adjustment process was performed by comparing the results with the relevant literature. A flood management plan has been previously developed and documented in this study area by the General Directorate of Water Manage-

ment (SYGM) of the Republic of Türkiye Ministry of Agriculture and Forestry in 2019 [37]. The parameters used for adjustment are shown in Table 3.

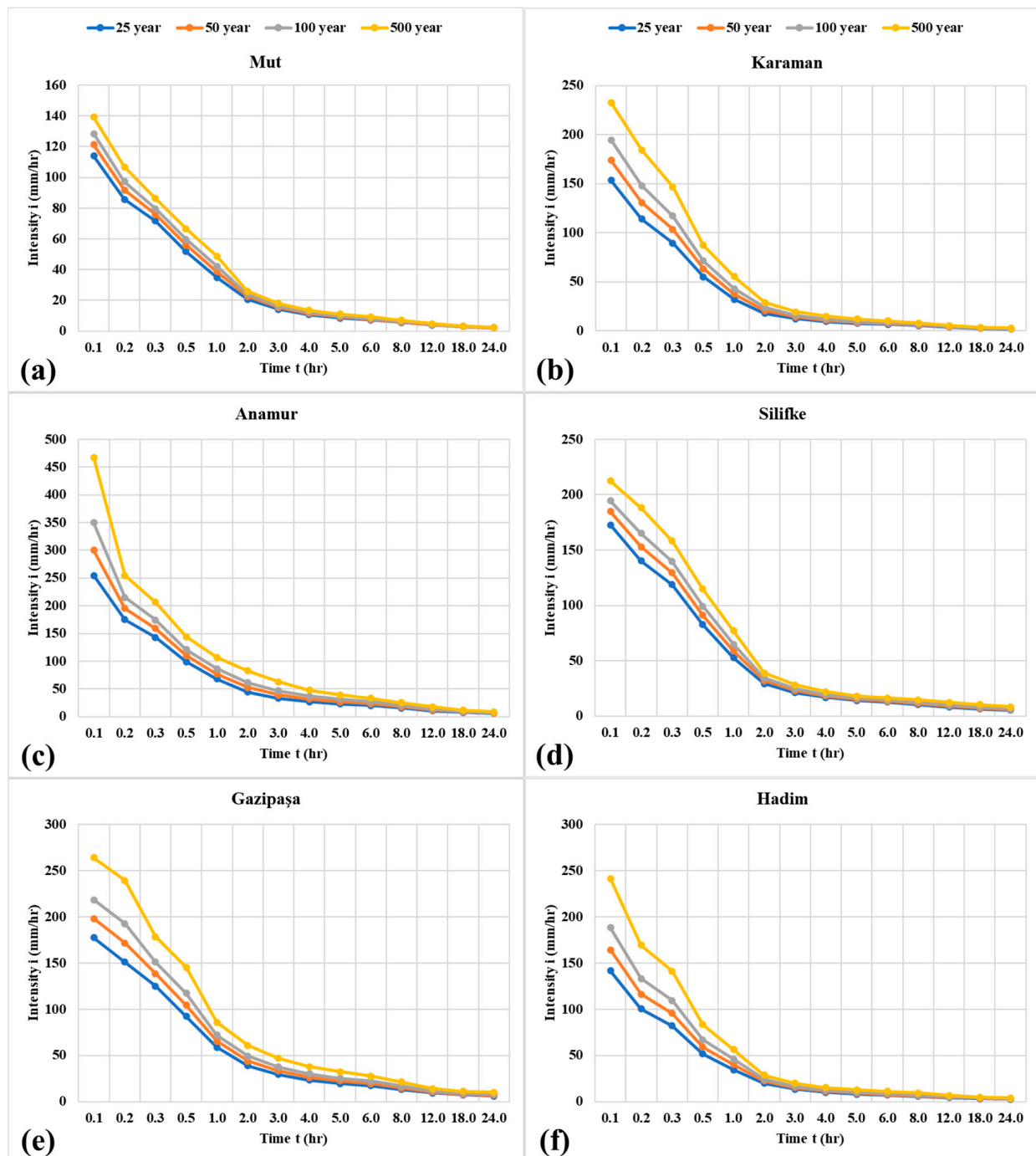


**Figure 6.** Intensity–duration–frequency (IDF) curves for stations of (a) Mut, (b) Karaman, (c) Anamur, (d) Silifke, (e) Gazipaşa, and (f) Hadim.

In the flood management plan, the 500-year, 100-year, and 50-year flood flow rates for the Göksu River were calculated as  $1831 \text{ m}^3/\text{s}$ ,  $1502 \text{ m}^3/\text{s}$ , and  $1345 \text{ m}^3/\text{s}$ , respectively, by using a stream gauge located downstream of the Göksu River Basin, as shown in Figure 1.

The calculated peak flow rates for the storm event using the HEC-HMS model and the 25-, 50-, 100-, and 500-year peak flow rates ( $Q_{25}$ ,  $Q_{50}$ ,  $Q_{100}$ , and  $Q_{500}$ ) calculated by [37] for the Göksu River Basin are given in results.

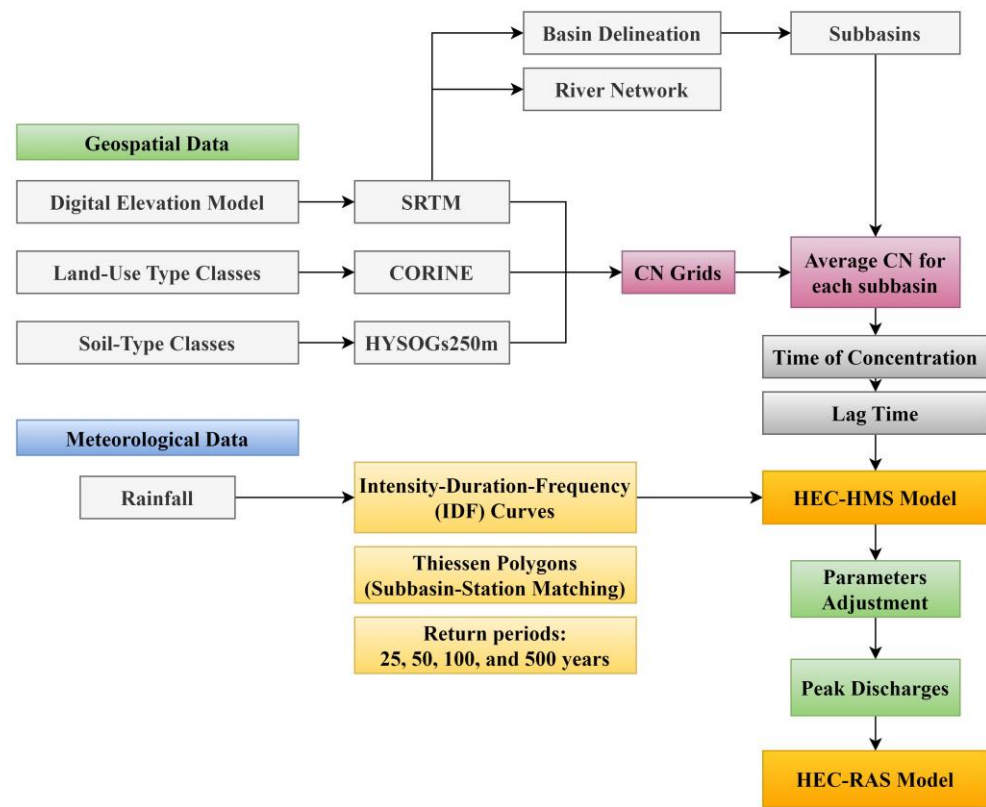


Figure 7. Flowchart of the HEC-HMS modeling part.

Table 3. Preferred modeling methods and adjusted parameters.

Hydrological Process	Method	Parameters	Unit	Fitting Value
Loss Method	SCS Curve Number	Initial Abstraction	mm	Automatic (0.2×)
		CN	unitless	Variable for each subbasin based on Table 2
		Impervious	%	10
Transform Method	Clark Unit Hydrograph	Time of concentration	h	Variable for each subbasin based on Table 2
		Storage coefficient	h	80
Routing Method	Lag	Lag time	min	Variable for each subbasin based on Table 2

#### 2.4. HEC-RAS Model Data and Runs

The HEC-RAS (Hydrological Engineering Centre River Analysis System) 5.0.7 software, introduced by the US Army Corps, is a widely utilized tool for flood modeling in hydrodynamic simulations and is freely accessible [45]. This model is capable of conducting 1D steady flow and 2D unsteady flow simulations for the transport of solids and water quality modeling [46]. It performs flow analysis using geometric and hydraulic calculation steps across a river network [47]. Users of the 2D HEC-RAS model have a choice of three equation sets: 2D diffusion wave equations (taken into account in this work), shallow water equations, which use the Eulerian–Lagrangian approach to solve for advection, or a new shallow water equations solver, which uses a Eulerian approach. The Navier–Stokes equations, which are the basis for the shallow water equations, are equations of conservation of mass and conservation of linear momentum, which continue to remain true under assumptions of shallow water breakdown, such as across a hydraulic jump [48]. The

shallow water equations are as follows for a horizontal bed with negligible Coriolis forces, frictional forces, and viscous forces:

$$\frac{\partial(\rho\eta)}{\partial t} + \frac{\partial(\rho\eta u)}{\partial x} + \frac{\partial(\rho\eta v)}{\partial y} = 0 \quad (2)$$

$$\frac{\partial(\rho\eta u)}{\partial t} + \frac{\partial}{\partial x} \left( \rho\eta^2 + \frac{1}{2}\rho g\eta^2 \right) + \frac{\partial(\rho\eta uv)}{\partial y} = 0 \quad (3)$$

$$\frac{\partial(\rho\eta v)}{\partial t} + \frac{\partial(\rho\eta uv)}{\partial x} + \frac{\partial}{\partial y} \left( \rho\eta v^2 + \frac{1}{2}\rho g\eta^2 \right) = 0 \quad (4)$$

The “ $\eta$ ” symbol here represents the total fluid column height (the instantaneous fluid depth as a function of  $x$ ,  $y$ , and  $t$ ), and the 2D vector  $(u, v)$  represents the fluid’s average horizontal flow velocity across the vertical column. Further,  $g$  stands for gravitational acceleration and for fluid density [49].

The first stage of hydraulic modeling with HEC-RAS involves high-resolution DEM data. The DEM data used in this study have a resolution of 5 m and were obtained using remote sensing techniques. The data were obtained from the Turkish General Directorate of Mapping. In hydraulic modeling, the DEM was cut to include the Silifke province of Mersin, which is the urban region in the basin, and the application area boundaries were determined. In the second stage, the calculation mesh dimensions were selected as 5 m to be compatible with the DEM. In the study, surface Manning “ $n$ ” values were determined using CORINE data from 2018 and the coefficients are defined for these surfaces in the literature [50]. Unsteady flow data were obtained from the HEC-HMS model as detailed in the previous subsection. Then, the river slope was determined in the GIS environment (0.0017) and the model was run with the boundary conditions defined as the inflow hydrograph and normal depth. Figure 8 shows the flowchart of HEC-RAS modeling.

### 2.5. Generation of the Flood Hazard Maps

People’s unconscious behaviors are the most common cause of injury or death during floods. People are typically unaware of the power of flowing water and endanger themselves and the people around them by unconsciously crossing current paths. Flood hazard levels are defined by the UK Department for Environment, Food and Rural Affairs, DEFRA [51], in its “Risk to People” guidance, which describes what people should and should not do in flood situations. The human guide recommends the hazard rating method in Equation (5) for determining the flood hazard level.

$$HR = d(v + n) + DF \quad (5)$$

where  $HR$  is hazard rating;  $d$  is flood depth (m);  $v$  is flow velocity (m/s);  $DF$  is the debris factor; and  $n$  is a constant of 0.5 [51,52]. Table 4 lists appropriate debris factors for different flood depths and velocities and the dominant land use and the level of flood hazard are determined according to the intervals in Table 5 [51].

**Table 4.** Debris factor selection [51].

Depth and Velocity	Pasture/Arable	Woodland	Urban
0.00–0.25 m	0	0	0
0.25–0.75 m	0	0.5	1
$d > 0.75$ m and/or $v > 2$	0.5	1	1

The four classes in Table 5 are obtained by determining the debris factor selected from Table 4 depending on the speed and/or depth change and writing the value of this factor into Equation (5). The flood velocity ( $v$ ) and flood depth ( $d$ ) expressions in Equation (5) must be defined for each element (pixel) on the surface where hydraulic modeling is performed.

Thus, HR values are determined for each element and the HR map is obtained by repeating the same process for all elements.

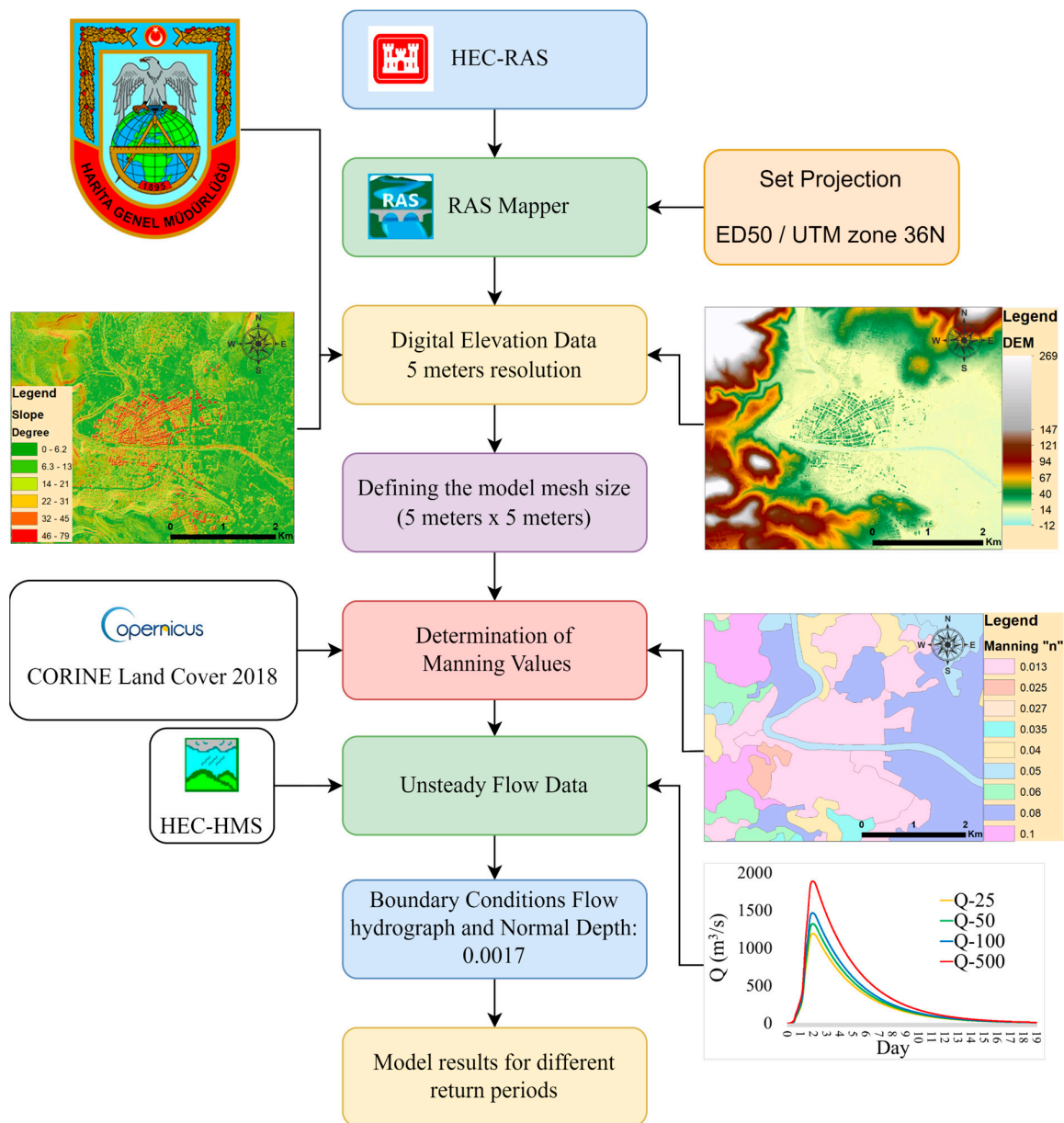


Figure 8. Flowchart of the HEC-RAS modeling.

Table 5. Determination of the flood hazard levels [51].

Thresholds for Flood Hazard Rating ( $HR = d \times (v + 0.5) + DF$ )	Flood Hazard Level	Woodland
<0.75	Low	Caution—"Flood zone with shallow flowing water or deep standing water"
0.75–1.25	Moderate	Dangerous for some (e.g., children)—"Danger: flood zone with deep or fast flowing water"
1.25–2.00	Significant	Dangerous for most people—"Danger: flood zone with fast flowing water"
>2	Extreme	Dangerous for all—"Extreme danger: flood zone with deep, fast flowing water"

### 3. Results

The HEC-HMS model was run using rainfall data with return intervals of 25, 50, 100, and 500 years. The peak flow rates obtained are given in Table 6 with values sourced from the literature and the HEC-HMS model. Additionally, hydrographs of the model simulations at the point where the stream gauge is located (Figure 1) are shown in Figure 9.

**Table 6.** Peak discharge for 25-, 50-, 100-, and 500-year return periods.

Peak Flow Rate Calculated by Using	Stream Flow Rate for Various Return Periods			
	Q25 (m <sup>3</sup> /s)	Q50 (m <sup>3</sup> /s)	Q100 (m <sup>3</sup> /s)	Q500 (m <sup>3</sup> /s)
HEC-HMS Model	1191.7	1321.2	1466.8	1888.3
Literature *	-	1345.0	1502.0	1831.0

\* SYGM (General Directorate of Water Management, in Turkish: Su Yönetimi Genel Müdürlüğü), (2019). “Doğu Akdeniz Basın Flood Management Plan” Report by Republic of Türkiye Ministry of Agriculture and Forestry—General Directorate of Water Management, Ankara, Türkiye, 1–827.

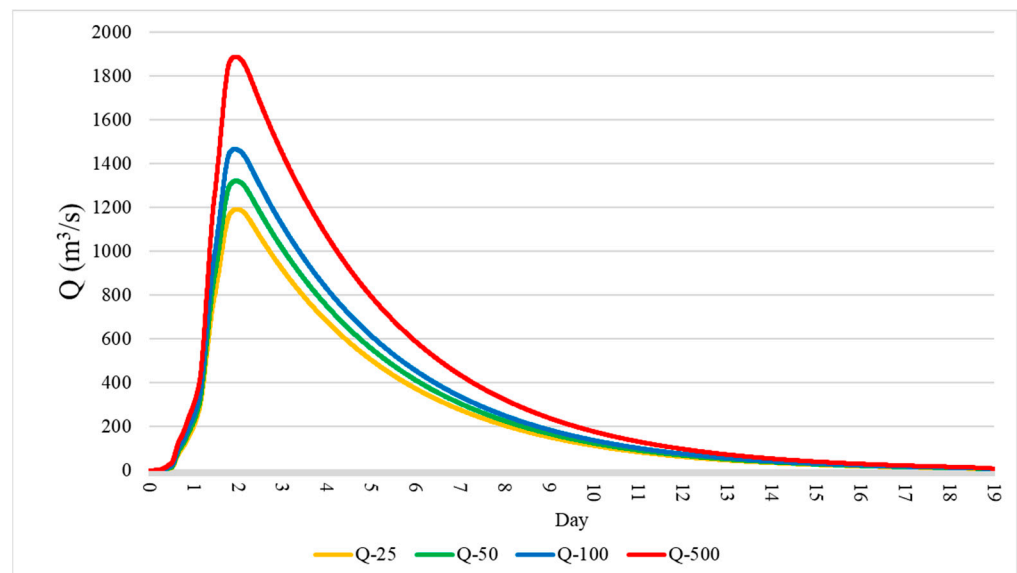


**Figure 9.** Hydrographs for 25-, 50-, 100-, and 500-year return periods.

Flood propagation maps in the study area belonging to the flow hydrographs obtained in Figure 9 are shown in Figure 10. In Figure 10, the flood propagation map shows that the flows in the return periods cannot fit into the river section and exceed the right and left banks, creating a hazard in the urban area. The right side of the study area is more affected by possible scenarios. The reasons for this are both the lower elevations of the regions on the right slopes and the fact that after the second bend of the river meanders on the upstream side, the river waters reach the right slope due to the centrifugal effect. Although water levels of up to 10 m were observed in some low-elevation areas in the middle section of the river in the study area, it was determined that the average water levels in the flood propagation area increased from 1.868, 1.916, and 1.928 m to 1.966 m from Q25 to Q500. While the average water velocities at these heights are 0.647 m/s in Q25, it increases to 0.725 m/s in Q500. While the speed values corresponding to the maximum depth are approximately 6 m/s, the speeds are quite low in areas where water spreads. This is due to the low slope of the area where the water spreads (up to 6 degrees on average, Figure 8). Table 7 shows flood propagation areas. The temporal changes of flood propagations can be followed in detail with the link in the “Supplementary Materials” section.

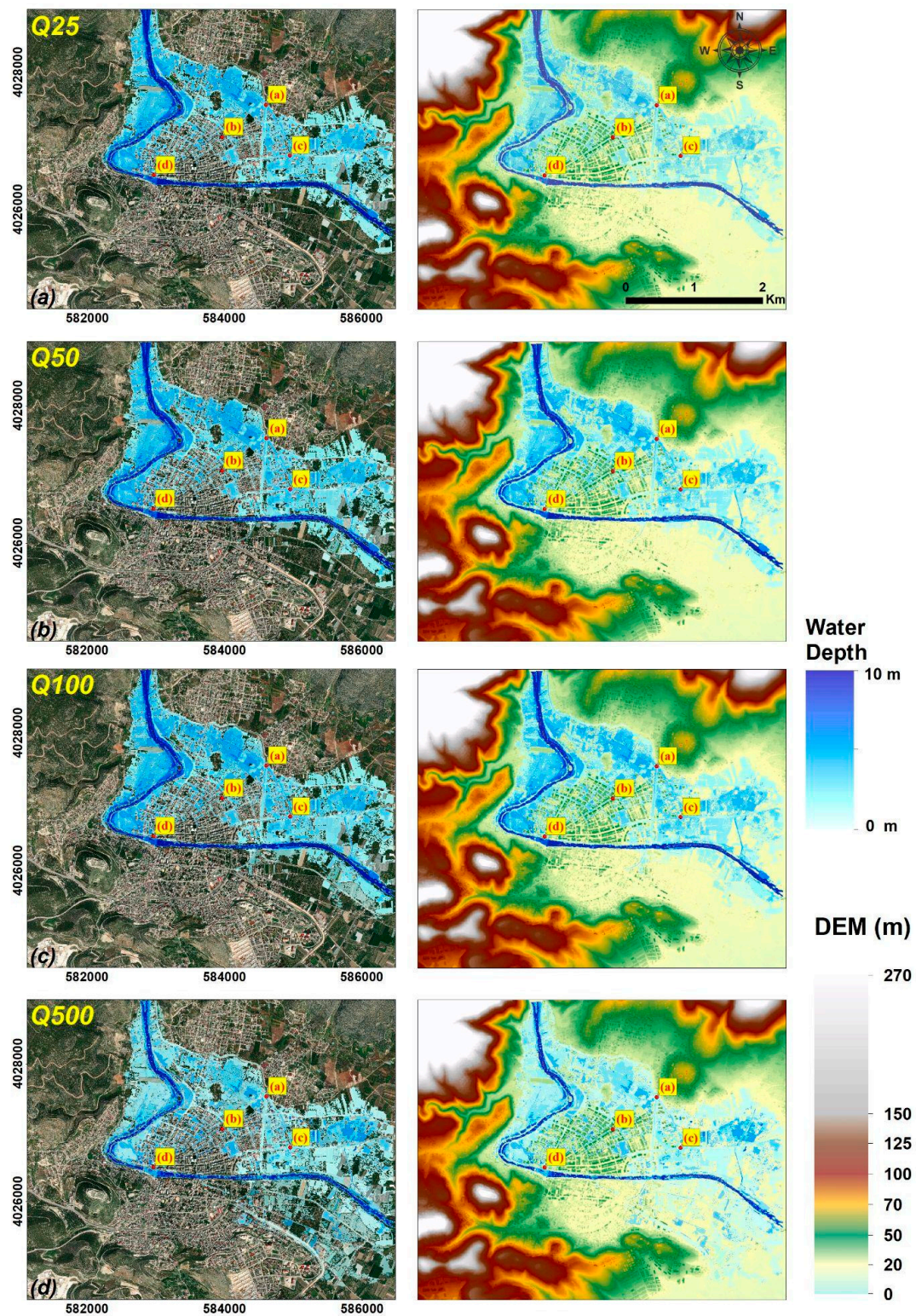


Figure 10. Flood propagation maps for 25- (a), 50- (b), 100- (c), and 500-year (d) return periods.

Table 7. Flood-inundated area (km<sup>2</sup>) for various return periods.

Return Period			
Q25	Q50	Q100	Q500
4.288	4.472	4.730	5.767

Table 7 shows that a large part of the study area (4.288 km<sup>2</sup>) was affected by floods starting from the Q25 flow rate. In addition, an area of 4.29% of the flood extent of the Q25 flow rate is seen in Q50. Similarly, an area of 10.3% of Q25 is seen in Q100, and an area of 34.5% is seen in Q500. Unfortunately, verification of the hydraulic model could not be conducted because there were no recorded data. However, considering the past flood points in Figure 1, it is seen that the model results give water distributions at similar points. This situation shows that the past floods of the region can be seen in return periods and the water distributions show the consistency of the results of the model. The hazard levels posed by these areas in the region were investigated using the DEFRA method. Figure 11 shows the hazard maps of the DEFRA method based on the relationship between flood depth and flow rates.

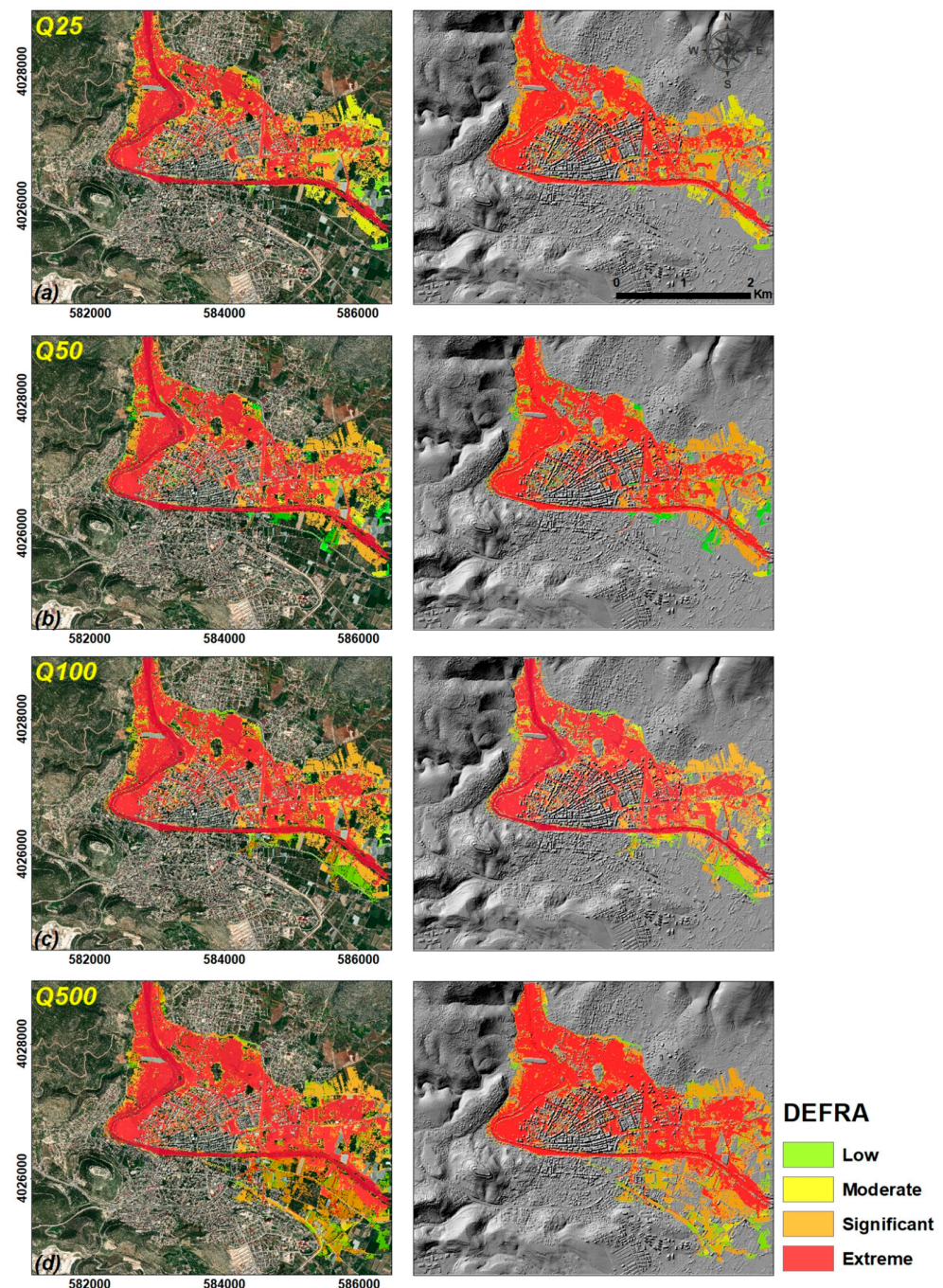


Figure 11. Flood hazard maps for 25- (a), 50- (b), 100- (c), and 500-year (d) return periods.

Raster data of water depth values and water velocities obtained after flood modeling with HEC-RAS were converted into debris factors using the Spatial Analysis Tools—Reclassify command in the ArcGIS 10.8.2 software. Then, Equation (5) was applied to these raster data with the help of the Spatial Analysis Tools—Raster Calculator command and hazard maps were obtained according to hazard classes according to the limit values in Table 5. When a large part of the study area is an urban area and high velocities due to slope are multiplied by high water levels, it can be seen that a large part of the area where the city center is located is classified as an extreme hazard. The lower right parts of the study area appear to be in low or medium danger due to the agricultural area and lower velocities and water levels.

#### 4. Discussion

There are many studies in both national and international bodies of literature with the combination of HEC-RAS and HEC-HMS applied in the Göksu River Basin [29,33]. The HEC-HMS model is fully automated; therefore, it has been frequently used in the literature in recent years [28]. Since the HEC-HMS model mainly simulates flow and compares it with measured data, it fills a significant gap in hydrological–hydraulic modeling studies. In this study, HEC-HMS results were found to be consistent with observed measurements.

Recent studies showed that DEM resolution is the parameter that directly determines the operating sensitivity in flood modeling [50]. For this purpose, 5 m high-resolution digital elevation model data were used in this study. In addition, processing surface details of buildings, riverbeds, etc., on DEM causes the study application area to turn into detailed topography. For this purpose, a digital surface model obtained by including layers such as buildings on a 5 m DEM was used in the study. The fact that this digital surface model was obtained by remote sensing techniques provides speed and economy and expresses the most up-to-date status of the topography. However, there are pixels with no height value at a few points of the river. These points were neglected in the modeling. Another critical issue pertains to Manning’s “n” values. The CORINE data used for this purpose (Figure 8) are the latest and most up to date, and roughness assignments are based on the literature [45,50]. Additionally, if Manning’s coefficients were selected manually (0.06), a 3.62% smaller area (4.31 km<sup>2</sup>) was determined by modeling the Q50 flow rate. This may sometimes have a positive or occasionally negative effect, but the error percentage is a size that should be considered. The use of the HEC-HMS structure in this study hybridizes it. In this respect, it is valuable and practical. Flood hydrograph peak flow rates obtained by HEC-HMS are compatible with studies in the literature. The peak flow difference between the HEC-HMS model and the report by the General Directorate of Water Management (SYGM) in the literature is presented in Table 6. It can be seen that the HEC-HMS results coincide with the results in the report. Therefore, these results indicate that the HEC-HMS model is a reliable and applicable model for flood modeling and flood hazard mapping. As a result of modeling, using the DEFRA method is vital in flood management studies before and in times of crisis and in prioritizing access to disaster victims (search and rescue) after floods [53].

Floods appear to be caused by the dimensional inadequacy of river sections to pass incoming flow rather than by structures or parameters affecting water flow hydrology. Water exceeding its cross section spreads rapidly in urban areas because the permeability of the channels or ground surfaces to be drained is very low. There are five bridges in the study area, including two pedestrian bridges. Model results show that bridge sections can pass incoming flood flows. Still, river sections are insufficient in regions where section narrowing occurs and inundates the left slope from upstream to downstream in the study area. Section-editing (cleaning) work needs to be performed, especially in narrow cross sections. To make the region resistant to flood danger, additional drainage channels can be built on the right slope of the river, and flow rates and velocities can be managed by reducing the base slope. In addition, meandering areas should be consid-

ered for the development of parks and gardens for recreational purposes and kept from construction plans.

## 5. Conclusions

In this study, flood propagation and flood hazard mapping of Göksu River Basin, Mersin, Türkiye, according to the DEFRA method were examined using GIS, HEC-HMS, and HEC-RAS. Maps were obtained for Q25, Q50, Q100, and Q500 floods, whose return periods represent standard recurrence periods. Flood maps showed that most of the area was highly affected by flood events during the 25-year return period (Q25).

The results of the modeling scenarios showed that the average water levels in the study area increased from 1.8 m to 2 m on average and the levels spread over an area from 4.28 km<sup>2</sup> to 5.76 km<sup>2</sup>. In addition, considering that the average velocity in the region was up to 0.7 m/s and the area studied was an urban area, in this case, the debris factor is equal to 1. It was determined that the majority of the flood-affected areas had an “Extreme” level of hazard (please see Table 5). This study is the first contribution to the literature regarding coupled hydrological and hydraulic modeling of the Göksu River Basin. The results can be used in basin management plans. Combining the hydrologic and hydraulic models used in this study can be applied to different flood-prone areas to generalize and check the reliability. To reduce the loss of goods and prevent possible damage caused by inundation, the models can be used to manage flood control and simulate inundation in real time. It is envisaged that flood effects in this region can be prevented by cleaning the river bottom and opening side channels. In addition, a large part of this floodplain should be forested and kept as agricultural land and/or parkland.

**Supplementary Materials:** HEC-RAS model videos: Flood inundated model for Q25: <https://www.youtube.com/watch?v=dhHkYgVg1uw&t=36s>; Flood inundated model for Q50: <https://www.youtube.com/watch?v=tPw96k4CqxE>; Flood inundated model for Q100: <https://www.youtube.com/watch?v=vynlK50epzk>; Flood inundated model for Q500: [https://www.youtube.com/watch?v=8L\\_51DY2V3o](https://www.youtube.com/watch?v=8L_51DY2V3o) (accessed on 16 January 2024).

**Author Contributions:** Conceptualization, S.G. and V.D.; methodology, İ.B.P., V.D. and N.B.; software, İ.B.P., V.D. and O.O.; validation, S.G., İ.B.P., O.O., N.B. and V.D.; visualization O.O., İ.B.P. and V.D.; resources, İ.B.P., S.G., V.D., O.O. and N.B.; writing—original draft preparation, İ.B.P., S.G., V.D., O.O. and N.B.; editing, İ.B.P., S.G., V.D., O.O. and N.B.; funding acquisition, N.B. and V.D. All authors have read and agreed to the published version of the manuscript.

**Funding:** This research was supported by the project SCORE (Smart Control of the Climate Resilience in European Coastal Cities) funded by the European Commission’s Horizon 2020 research and innovation program under grant agreement No. 101003534.

**Institutional Review Board Statement:** Not applicable.

**Informed Consent Statement:** Not applicable.

**Data Availability Statement:** The data presented in this study are available on request from the corresponding author.

**Acknowledgments:** The authors would like to thank the Turkish State Hydraulic Works (DSI), the Turkish State Meteorological Service (TSMS), and the General Directorate of Mapping and their employees for the data they provided.

**Conflicts of Interest:** The authors declare no conflicts of interest.

## References

1. Cui, P.; Peng, J.; Shi, P.; Tang, H.; Ouyang, C.; Zou, Q.; Liu, L.; Li, C.; Lei, Y. Scientific Challenges of Research on Natural Hazards and Disaster Risk. *Geogr. Sustain.* **2021**, *2*, 216–223. [[CrossRef](#)]
2. EM-DAT: *The Emergency Events Database*; Universite Catholique de Louvain: Brussels, Belgium. Available online: <https://www.emdat.be/> (accessed on 1 January 2024).
3. Das, S.; Pardeshi, S.D. Comparative Analysis of Lineaments Extracted from Cartosat, SRTM and ASTER DEM: A Study Based on Four Watersheds in Konkan Region, India. *Spat. Inf. Res.* **2018**, *26*, 47–57. [[CrossRef](#)]

4. Ahmad, D.; Afzal, M. Flood Hazards and Livelihood Vulnerability of Flood-Prone Farm-Dependent Bait Households in Punjab, Pakistan. *Environ. Sci. Pollut. Res.* **2022**, *29*, 11553–11573. [[CrossRef](#)]
5. Fernández, D.S.; Lutz, M.A. Urban Flood Hazard Zoning in Tucumán Province, Argentina, Using GIS and Multicriteria Decision Analysis. *Eng. Geol.* **2010**, *111*, 90–98. [[CrossRef](#)]
6. Ertan, A.; Özalkan, E.; Karaman, M. Determination of Flood Areas in Geographic Information Systems Platform Using Analytical Hierarchy Process: A Case Study in Çanakkale—Karamenderes Basin. *J. Res. Atmos. Sci.* **2021**, *3*, 1–9. [[CrossRef](#)]
7. Selçuk, L.; Sağlam Selçuk, A.; Kasapoğlu, D. Urban Flood Susceptibility Assessment of Central Districts of Van Province, Turkey, Using Geographic Information System (GIS)-Based Multi Criteria Decision Analysis (MCDA). *Bull. Earth Sci. Appl. Res. Cent. Hacettepe Univ. Coğrafi* **2016**, *37*, 1–17. [[CrossRef](#)]
8. Billa, L.; Shattri, M.; Mahmud, A.R.; Ghazali, A.H. Comprehensive Planning and the Role of SDSS in Flood Disaster Management in Malaysia. *Disaster Prev. Manag. An Int. J.* **2006**, *15*, 233–240. [[CrossRef](#)]
9. Tehrani, M.S.; Lee, M.J.; Pradhan, B.; Jebur, M.N.; Lee, S. Flood Susceptibility Mapping Using Integrated Bivariate and Multivariate Statistical Models. *Environ. Earth Sci.* **2014**, *72*, 4001–4015. [[CrossRef](#)]
10. Swain, K.C.; Singha, C.; Nayak, L. Flood Susceptibility Mapping through the GIS-AHP Technique Using the Cloud. *ISPRS Int. J. Geo-Inf.* **2020**, *9*, 720. [[CrossRef](#)]
11. Alarifi, S.S.; Abdelkareem, M.; Abdalla, F.; Alotaibi, M. Flash Flood Hazard Mapping Using Remote Sensing and GIS Techniques in Southwestern Saudi Arabia. *Sustainability* **2022**, *14*, 14145. [[CrossRef](#)]
12. Roy, D.K.; Sarkar, T.K.; Kamar, S.S.A.; Goswami, T.; MuktaDir, M.A.; Al-Ghobari, H.M.; Alataway, A.; Dewidar, A.Z.; El-Shafei, A.A.; Mattar, M.A. Daily Prediction and Multi-Step Forward Forecasting of Reference Evapotranspiration Using LSTM and Bi-LSTM Models. *Agronomy* **2022**, *12*, 594. [[CrossRef](#)]
13. Beden, N.; Ulke Keskin, A. Estimation of the Local Financial Costs of Flood Damage with Different Methodologies in Unye (Ordu), Turkey. *Nat. Hazards* **2021**, *108*, 2835–2854. [[CrossRef](#)]
14. Tsakiris, G. Flood Risk Assessment: Concepts, Modelling, Applications. *Nat. Hazards Earth Syst. Sci.* **2014**, *14*, 1361–1369. [[CrossRef](#)]
15. Scharffenberg, J.M.; Fleming, J.M. *Hydrologic Modeling System HEC-HMS User's Manual Version 3.5*; Hydrologic Engineering Center: Davis, CA, USA, 2010.
16. Yu, X.; Zhang, J. The Application and Applicability of HEC-HMS Model in Flood Simulation under the Condition of River Basin Urbanization. *Water* **2023**, *15*, 2249. [[CrossRef](#)]
17. Kazezyilmaz-Alhan, C.M.; Yalçın; Javanshour, K.; Aytakin, M.; Gülbaz, S. A Hydrological Model for Ayamama Watershed in Istanbul, Turkey, Using HEC-HMS. *Water Pract. Technol.* **2021**, *16*, 154–161. [[CrossRef](#)]
18. Liu, W.C.; Hsieh, T.H.; Liu, H.M. Flood Risk Assessment in Urban Areas of Southern Taiwan. *Sustainability* **2021**, *13*, 3180. [[CrossRef](#)]
19. Janicka, E.; Kanclerz, J.; Agaj, T.; Gizińska, K. Comparison of Two Hydrological Models, the HEC-HMS and Nash Models, for Runoff Estimation in Michałówka River. *Sustainability* **2023**, *15*, 7959. [[CrossRef](#)]
20. Khan, M.Y.A.; ElKashouty, M.; Subyani, A.M.; Tian, F. Flash Flood Assessment and Management for Sustainable Development Using Geospatial Technology and WMS Models in Abha City, Aseer Region, Saudi Arabia. *Sustainability* **2022**, *14*, 10430. [[CrossRef](#)]
21. Ibrahim-Bathis, K.; Ahmed, S.A. Rainfall-Runoff Modelling of Doddahalla Watershed—An Application of HEC-HMS and SCN-CN in Ungauged Agricultural Watershed. *Arab. J. Geosci.* **2016**, *9*, 170. [[CrossRef](#)]
22. Wang, M.; Zhang, L.; Baddoo, T.D. Hydrological Modeling in A Semi-Arid Region Using HEC-HMS. *J. Water Resour. Hydraul. Eng.* **2016**, *5*, 105–115. [[CrossRef](#)]
23. Tang, Y.; Leon, A.S.; Kavvas, M.L. Impact of Size and Location of Wetlands on Watershed-Scale Flood Control. *Water Resour. Manag.* **2020**, *34*, 1693–1707. [[CrossRef](#)]
24. Jin, H.; Liang, R.; Wang, Y.; Tumula, P. Flood-Runoff in Semi-Arid and Sub-Humid Regions, a Case Study: A Simulation of Jianghe Watershed in Northern China. *Water* **2015**, *7*, 5155–5172. [[CrossRef](#)]
25. Halwatura, D.; Najim, M.M.M. Application of the HEC-HMS Model for Runoff Simulation in a Tropical Catchment. *Environ. Model. Softw.* **2013**, *46*, 155–162. [[CrossRef](#)]
26. De Silva, M.M.G.T.; Weerakoon, S.B.; Herath, S. Modeling of Event and Continuous Flow Hydrographs with HEC-HMS: Case Study in the Kelani River Basin, Sri Lanka. *J. Hydrol. Eng.* **2014**, *19*, 800–806. [[CrossRef](#)]
27. Alfy, M. El Assessing the Impact of Arid Area Urbanization on Flash Floods Using GIS, Remote Sensing, and HEC-HMS Rainfall-Runoff Modeling. *Hydrol. Res.* **2016**, *47*, 1142–1160. [[CrossRef](#)]
28. Abdessamed, D.; Abderrazak, B. Coupling HEC-RAS and HEC-HMS in Rainfall-Runoff Modeling and Evaluating Floodplain Inundation Maps in Arid Environments: Case Study of Ain Sefra City, Ksour Mountain. SW of Algeria. *Environ. Earth Sci.* **2019**, *78*, 586. [[CrossRef](#)]
29. Gül, G.O.; Harmancıoğlu, N.; Gül, A. A Combined Hydrologic and Hydraulic Modeling Approach for Testing Efficiency of Structural Flood Control Measures. *Nat. Hazards* **2010**, *54*, 245–260. [[CrossRef](#)]
30. Hashemyan, F.; Khaleghi, M.; Kamyar, M. Combination of HEC-HMS and HEC-RAS Models in GIS in Order to Simulate Flood (Case Study: Khoshke Rudan River in Fars Province, Iran). *Res. J. Recent Sci. Res. J. Recent Sci.* **2015**, *4*, 122–127.

31. Yamani, K.; Hazzab, A.; Sekkoum, M.; Slimane, T. Mapping of Vulnerability of Flooded Area in Arid Region. Case Study: Area of Ghardaïa-Algeria. *Model. Earth Syst. Environ.* **2016**, *2*, 147. [CrossRef]
32. Mai, D.; De Smedt, F. A Combined Hydrological and Hydraulic Model for Flood Prediction in Vietnam Applied to the Huong River Basin as a Test Case Study. *Water* **2017**, *9*, 879. [CrossRef]
33. Namara, W.G.; Damisse, T.A.; Tufa, F.G. Application of HEC-RAS and HEC-GeoRAS Model for Flood Inundation Mapping, the Case of Awash Bello Flood Plain, Upper Awash River Basin, Oromiya Regional State, Ethiopia. *Model. Earth Syst. Environ.* **2022**, *8*, 1449–1460. [CrossRef]
34. Koç, G.; Thieken, A.H. The Relevance of Flood Hazards and Impacts in Turkey: What Can Be Learned from Different Disaster Loss Databases? *Nat. Hazards* **2018**, *91*, 375–408. [CrossRef]
35. Koç, G.; Petrow, T.; Thieken, A.H. Analysis of the Most Severe Flood Events in Turkey (1960–2014): Which Triggering Mechanisms and Aggravating Pathways Can Be Identified? *Water* **2020**, *12*, 1562. [CrossRef]
36. Buldur, A.D.; Pinar, A.; Başaran, A. Flood of Göksu River Dated 05-07 March 2004 and Its Impact on Silifke. *J. Selçuk Univ. Soc. Sci. Inst.* **2007**, *17*, 139–160.
37. SYGM. *Eastern Mediterranean Basin Flood Management Plan*; T.C. Tarım Ve Orman Bakanlığı Su Yönetimi Genel Müdürlüğü: Ankara, Turkey, 2019.
38. AFAD Planning and Risk Reduction Department. *Provincial Disaster Risk Reduction Plan*; AFAD Planning and Risk Reduction Department: Mersin, Turkey, 2021.
39. Koç, G.; Thieken, A.H. Societal and Economic Impacts of Flood Hazards in Turkey—An Overview. *E3S Web Conf.* **2016**, *7*, 05012. [CrossRef]
40. Jarvis, A.; Guevara, E.; Reuter, H.I.; Nelson, A.D. Hole-Filled SRTM for the Globe: Version 4: Data Grid, CGIAR Consortium for Spatial Information. Available online: <http://srtm.csi.cgiar.org/> (accessed on 9 June 2023).
41. Büttner, G.; Kosztra, B.; Maucha, G.; Pataki, R.; Kleeschulte, S.; Hazeu, G.W.; Vittek, M.; Schroder, C.; Littkopf, A. *Copernicus Land Monitoring Service—CORINE Land Cover User Manual*; Copernicus Publications: Bonn, Germany, 2021.
42. Ross, C.W.; Prihodko, L.; Anchang, J.; Kumar, S.; Ji, W.; Hanan, N.P. HYSOGs250m, Global Gridded Hydrologic Soil Groups for Curve-Number-Based Runoff Modeling. *Sci. Data* **2018**, *5*, 180091. [CrossRef]
43. Maidment, D.R. *Arc Hydro: GIS for Water Resources*; ESRI, Inc.: Redlands, CA, USA, 2002.
44. Natural Resources Conservation Service (NRCS). Time of Concentration (Chapter 15). In *Hydrology National Engineering Handbook*; Natural Resources Conservation Service (NRCS): Washington, DC, USA, 2010; pp. 1–29.
45. Hadi, Z.N.; Almansori, N.J.H. Estimation of Manning Coefficient for the Section between Al-Hindiya Barrage and Al-Kufa Barrage Utilizing HEC-RAS. *Mater. Today Proc.* **2023**, *80*, 2595–2601. [CrossRef]
46. Demir, V.; Beden, N.; Ülke, A. Review and Comparison of Flood Modeling Methods. *Eur. J. Sci. Technol.* **2021**, *2021*, 1013–1021. [CrossRef]
47. Lea, D.; Yeonsu, K.; Hyunuk, A. Case Study of HEC-RAS 1D-2D Coupling Simulation: 2002 Baeksan Flood Event in Korea. *Water* **2019**, *11*, 2048. [CrossRef]
48. Acheampong, J.N.; Gyamfi, C.; Arthur, E. Impacts of Retention Basins on Downstream Flood Peak Attenuation in the Odaw River Basin, Ghana. *J. Hydrol. Reg. Stud.* **2023**, *47*, 101364. [CrossRef]
49. U.S. Army Corps of Engineering. *HEC-RAS 5.0 Supplemental to User's Manual*; U.S. Army Corps of Engineering: Huntsville, AL, USA, 2018.
50. Papaioannou, G.; Efstratiadis, A.; Vasiliades, L.; Loukas, A.; Papalexioiu, S.M.; Koukouvinos, A.; Tsoukalas, I.; Kossieris, P. An Operational Method for Flood Directive Implementation in Ungauged Urban Areas. *Hydrology* **2018**, *5*, 24. [CrossRef]
51. Defra. Environment Agency Flood Risks to People—Phase 2—FD2321/TR2 Guidance Document. 2006; 91p. Available online: [https://assets.publishing.service.gov.uk/media/602bbc3de90e07055f646148/Flood\\_risks\\_to\\_people\\_-\\_Phase\\_2\\_Guidance\\_Document\\_Technical\\_report.pdf](https://assets.publishing.service.gov.uk/media/602bbc3de90e07055f646148/Flood_risks_to_people_-_Phase_2_Guidance_Document_Technical_report.pdf) (accessed on 9 June 2023).
52. van Alphen, J.; Passchier, R. Atlas of Flood Maps, examples from 19 European countries, USA and Japan, Ministry of Transport, Public Works and Water Management, The Hague, Netherlands, prepared for EXCIMAP. 2007. Available online: <http://ec.europa.eu/environment/water/flood%20risk/flood%20atlas/index.htm> (accessed on 28 January 2024).
53. Priest, S.J.; Parker, D.J.; Tapsell, S.M. Modelling the Potential Damage-Reducing Benefits of Flood Warnings Using European Cases. *Environ. Hazards* **2011**, *10*, 101–120. [CrossRef]

**Disclaimer/Publisher's Note:** The statements, opinions and data contained in all publications are solely those of the individual author(s) and contributor(s) and not of MDPI and/or the editor(s). MDPI and/or the editor(s) disclaim responsibility for any injury to people or property resulting from any ideas, methods, instructions or products referred to in the content.